IEEES – 2017 – 112

Numerical Studies of a 3D DMFC Short-Stack

David Ouellette, Can Ozgur Colpan

Dokuz Eylul University, Faculty of Engineering, Mechanical Engineering Department, Tinaztepe, Buca, Izmir, 35397, Turkey

E-mails: ouellette.d@gmail.com ; ozgur.colpan@deu.edu.tr

Abstract

One of the primary challenges in fuel cell stack models, is the lack of numerical methods and computational resources available to handle a full-scale stack geometry (which can often have ~10-100 single cells stacked in series) to at least the same grid resolution and detailed physics as could be obtained in an equivalently detailed single cell model. To help resolve this challenge, a 3D modelling approach is proposed, and applied to a 5-cell direct methanol fuel cell (DMFC) short-stack. In this approach, the flow fields, backing layers and membranes are solved numerically in a 3D manner, whereas the electrochemical performance is solved analytically. This approach allowed for the detailed physics to be incorporated into the model without the requirement of a high mesh density within the MEA. Thus softening the computational load. Since it is well-known that non-uniform flow distributions within the stack's cells and within the MEA can lead to accelerated aging of the fuel cell components, a parametric study on the anode and cathode flow rates, and methanol concentrations are examined numerically. The model was used to shed light onto the mechanisms that lead to non-uniform flow behaviour within the stack's cells; help identify methods to maintain a uniform flow and concentration distribution within the stack; and to provide methods to minimize methanol crossover to the cathode.

Keywords: Short-stack, DMFC, flow distribution, stack model.

I. Introduction

Direct methanol fuel cell (DMFC) is one of the low temperature fuel cell types that can be mainly used in grid-independent portable applications. Methanol, being in the liquid form, is easy to achieve and store and has high energy density. However, being a toxic material, a special care has to be given in the selection and design of the methanol containers. DMFC technology has also some challenges towards its widespread commercialization such as low performance due to the slow reactions at the electrodes and methanol crossover problem and high cost of catalyst. In a conventional DMFC, Pt-Ru/C, Pt-C, Nafion® 115, carbon paper or cloth, and graphite are used as the materials of the anode catalyst, cathode catalyst, membrane, backing layer, and flow field respectively. The Pt loadings of anode and cathode are generally taken as 2.7 mg/cm^2 and 2 mg/cm^2, respectively. In a report by Zelenay (2012), they gave their project performance target for a DMFC as 0.15 $A{\cdot}cm^2$ at 0.6 V. They reported that they achieved 0.56 V at 0.15 $A{\cdot}cm^{-2}$ with the following design and operating conditions: Pt:Ru atomic ratio of 1:4 (JMFC's advanced anode catalyst), anode catalyst loading of 1.0 $mg_{pt}{\cdot}cm^{-2}$, Pt/C catalyst loading of 1.5 $mg_{pt}{\cdot}cm^{-2}$, Nafion® 115 membrane, cell temperature of 88 °C, methanol concentration of 0.6 M, air in the cathode. There is still ongoing research on the selection of materials for catalysts, catalyst supports and membranes, and other designs to improve the performance of DMFCs (e.g. Brandão et al. (2010), Casalegno et al. (2011), Colpan et al. (2017), Liu et al. (2016), Mondal et al. (2015) Seo and Lee (2010)).

DMFC stack, which is formed bringing many single cells together, can be designed in different ways. These differences arise from using different flow patterns and flow field types in the stack. U shape (inlet and outlet are at the same side of the stack) or Z shape flow pattern (inlet and outlet are at the opposite sides of the stack) can be selected (Barbir, 2012). A suitable configuration of a flow field should be selected, which yields optimum pressure drop, uniform reactant distribution, and effective removal of the products. Depending on the active area, generally, a variation of a serpentine, parallel or pin design are generally used as the flow field type. In a recent study (e.g. Ozden et al. (2016)), different bio-inspired flow field designs were used in either one side or both sides of the fuel cell for performance comparison purposes. In addition to the performance, the durability is a key indicator for the success of a stack. Zelenay (2012) reported that advanced anode catalyst based catalyst coated membranes (with an active area of 50 cm^2) were used in a 10-cell stack and tested in SFC Energy. They reached the maximum stack voltage after 70 hours of operation and a decay rate of 19 μV/h (per cell) was seen in around 2,800 hours of operation.

Mathematical models of fuel cells have been developed in cell, stack, and system level at different level of complexity in the literature. In cell level modeling, the aim is to model a repeat element, which is generally taken as the portion of the DMFC around of a single channel found in the middle of the flow field,

or the complete single cell containing the geometrical details of the flow field. In stack-level, the geometry selected for modeling generally includes the geometrical details of the flow pattern and configuration. In system-level, generally, fuel cell and other components are considered as black box (0-D modeling approach). In cell and stack-level, analytical solutions are generally applied if 0D or 1D modeling technique is applied and numerical solutions are generally used for 2D or 3D (single phase or two-phase) modeling approaches.

Although there are many studies on hydrogen fueled proton exchange membrane fuel stacks in the literature (e.g. Chang et al. (2007), Fang et al. (2009), Kvesić et al. (2012), Kong and Khambadkone (2009), Liu et al. (2006), Philipps and Ziegler (2008), Musio et al. (2011), Shimpalee et al. (2009)), There are some studies on the modeling of DMFC stack in the literature. For example, Kablou (2012) designed and manufactured a five-cell flowing electrolyte-DMFC stack having a parallel serpentine flow field design and U-type manifold configuration. He used an analytical approach, namely "Hardy Cross" method, for this purpose. He showed that the flowing electrolyte reduces the methanol crossover effectively and enhances the performance of the stack. Argyropoulos et al. (2000) developed a two-phase DMFC stack model to describe its hydraulic behavior. Using this model, pressure drop of each cell and flow distribution through the internal manifolds were found. Wang et al. (2008) developed a DMFC stack model using adaptive network-based fuzzy inference systems method. The main inputs of their model were temperature, methanol concentration and current; whereas the cell voltage was the output. They showed the importance of selecting the values of methanol concentration and temperature to get high values of fuel utilization. Scott et al. (2000) developed a DMFC stack model to predict several important performance parameters such as the stack voltage, overall system pressure, and fluid distribution from the manifolds.

The literature survey conducted showed that although some DMFC stack models were developed, according to the authors' knowledge, a model including a detailed stack geometry and transport phenomena is not found. For this purpose, a 3D modelling approach is applied to a 5-cell DMFC stack. Pressure and velocity distributions as well as methanol and oxygen concentration distributions for different anode and cathode inlet flow rates are studied.

II. Computational model

II.1. Computational domain

The three dimensional computational domain consists of a 5-cell short stack in a Z-type manifold, as shown in Fig. 1a. Each cell has an active surface area of 25 cm^2, whereas each anode flow field consists of a parallel serpentine design (5 channels; Fig. 1b), and each cathode flow field consists of a straight parallel design (25 channels; Fig. 1b). The MEA, shown in the sub-figure of Fig. 1a, consists of an anode and cathode backing layer (ABL and CBL, respectively), catalyst layer (ACL and CCL, respectively; each considered as and interface), and a membrane (considered to be completely liquid equilibrated). Methanol and oxygen are supplied in a cross-flow configuration.

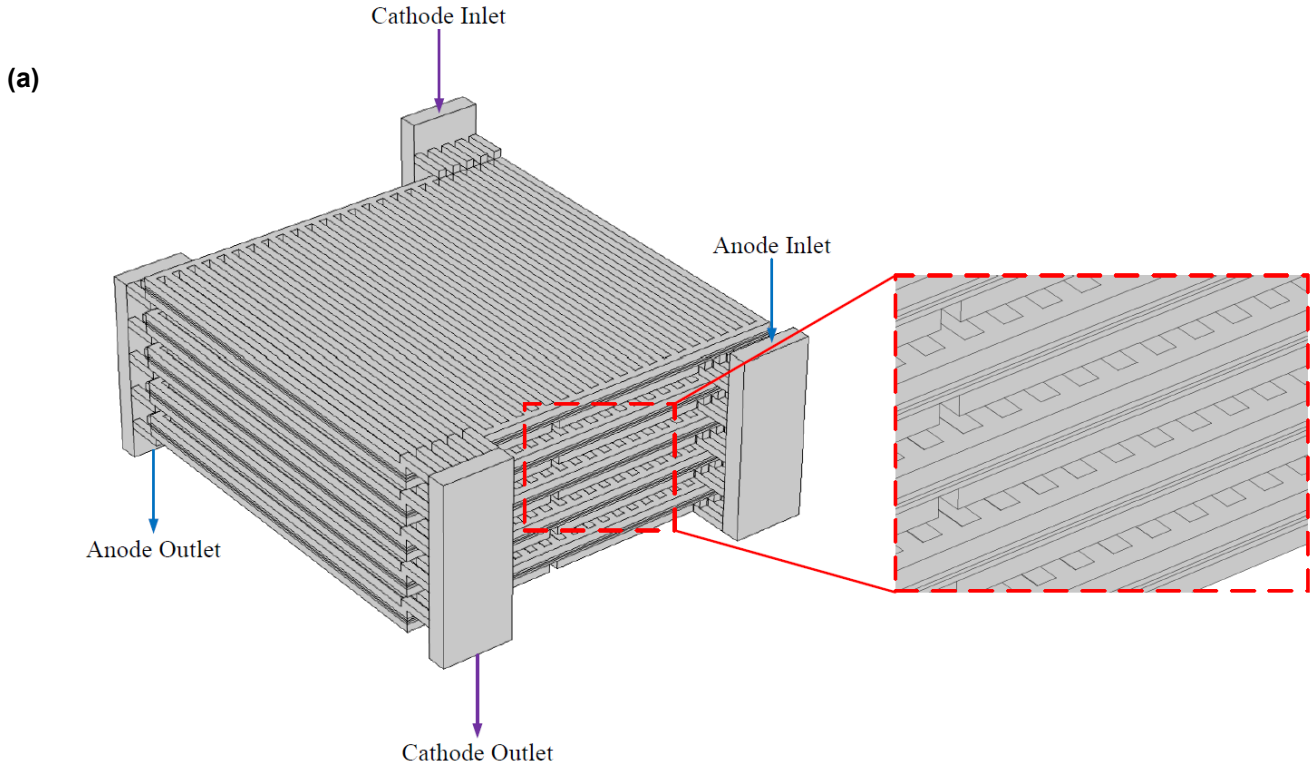

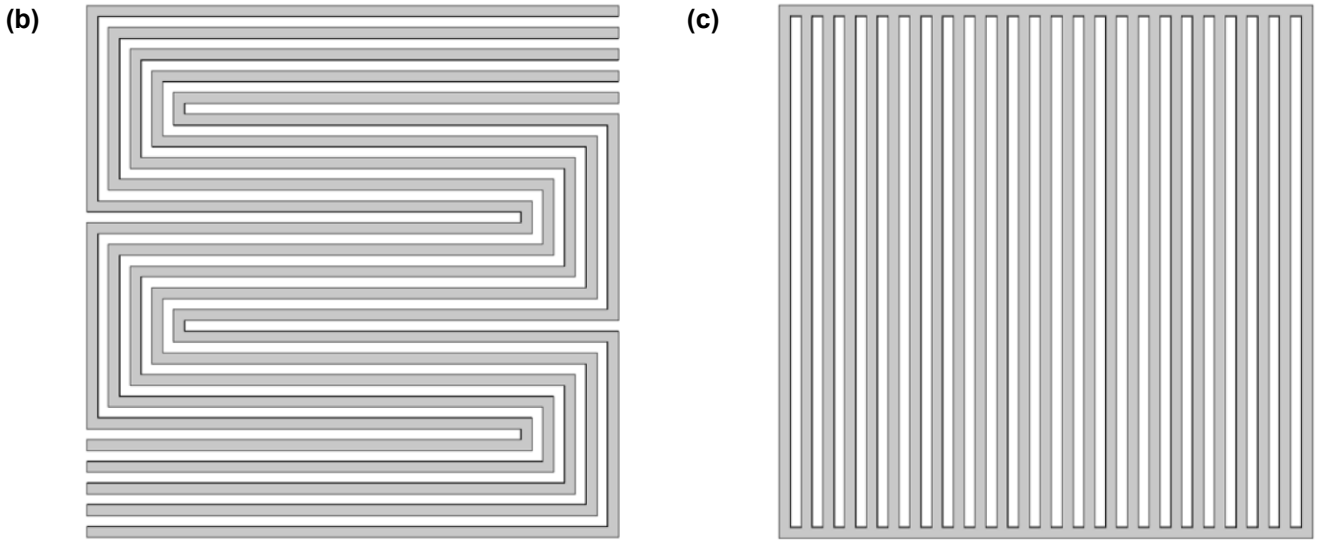

Fig. 1: (a) Computational domain of the entire 5-cell short stack used in this study. The sub-figure shows the considered MEA. (b) and (c) represent the anode and cathode flow fields, respectively.

II.2. Modeling assumptions

To model the previously described domain, the following assumptions were made:

- The fuel cell operates under steady state, isothermal and single phase conditions.
- All fluids are ideal and exist in equilibrium with one another.
- Each media is homogeneous and isotropic.
- The membranes are impermeable to the gaseous phase.
- All crossed over methanol is fully consumed at the cathode catalyst layer.
- The mass transfer within the porous layers are diffusion-dominant.

II.3. Governing equations

Three conservation equations are used in this 3D, steady state, isothermal and single phase model: the conservation of mass (Eq. (1)), momentum (Eq. (2)), and species (Eq. (3); applied to methanol and oxygen).

$$\rho\left(\nabla\cdot\mathbf{u}\right)=S_{gen} \tag{1}$$

$$\frac{\rho\mathbf{u}}{\varepsilon^2}\left(\nabla\cdot\mathbf{u}\right)=\nabla\cdot\left[-P\mathbf{I}+\frac{\mu}{\varepsilon}\left\langle\left(\nabla\cdot\mathbf{u}\right)+\left(\nabla\cdot\mathbf{u}\right)^{T}\right\rangle-\frac{2\mu}{3\varepsilon}\left(\nabla\cdot\mathbf{u}\right)\mathbf{I}\right] \tag{2}$$

$$\nabla\cdot\left[-D_i^k\left(\nabla C_i^k\right)\right]+\mathbf{u}\left(\nabla C_i^k\right)=S_{gen,i}^k \tag{3}$$

In Eq. (1), ρ is the mass density, $\mathbf{u}$ is the superficial velocity within the porous layers, and S_{gen} is the mass source term associated with the chemical reactions within the catalyst layers. Within Eq. (2), ε is the porosity, P is the pressure, $\mathbf{I}$ is the identity matrix, μ is the dynamic viscosity, and K is the absolute permeability. Within Eq. (3), D is the molecular diffusivity (corrected for the porous structure via the Bruggeman equation), C is the molar concentration, and $S_{gen,i}^k$ is the molar source term of an arbitrary species k in phase i. It should be noted, that for simplicity, convection is only considered within the channels.

II.4. Electrochemical relationships

To calculate each of the cell's voltage, V_{cell}, reversible cell voltage, V_{rev}, is subtracted from each of the respective cell's loss mechanisms (i.e.: the anode [a] and cathode [c] activation [η_{act}] polarizations, as well as the cell's Ohmic polarization [η_Ω]), as given by Eq. (4).

$$V_{cell}=V_{rev}-\eta_{act,a}-\eta_{act,c}-\eta_\Omega \tag{4}$$

The anode activation polarization is estimated from the anodic Meyers-Newman (non-Tafel) equation (Eq. (5)), whereas the cathode activation polarization is obtained from the Tafel equation (Eq. (6)) (Ozden et al. (2016)).

$$\eta_a=\frac{\bar{R}T}{\alpha_a F}\ln\left[\frac{i\cdot C_{l,ACL}^M}{i_{a,ref}\cdot C_{l,ACL}^M-i\cdot K_a}\right] \tag{5}$$

$$\eta_c=\frac{\bar{R}T}{\alpha_c F}\ln\left[\left(\frac{i+i_{xover}}{i_{c,ref}}\right)\cdot\left(\frac{C_{g,ref}^{O_2}}{C_{g,CCL}^{O_2}}\right)\right] \tag{6}$$

Here, $\bar{R}$ is the universal gas constant, T is the cell temperature, α is the charge transfer coefficient, F is Faraday's constant, K_a is the methanol oxidation reaction constant, i_{xover} is the crossover current density (obtained from Eq. (7). The terms within the square brackets represents the methanol's molar permeation rate to the cathode, accounting for the diffusive and electro-osmotic transport mechanisms) and i_{ref} is the reference exchange current density. The methanol and oxygen concentrations are measured at the CL surface, with the subscript *ref* referring to the reference concentration.

$$i_{xover} = 6F\left[-D_e^M\left(\nabla C_l^M\right)+\left(\frac{n_d^{H_2O}}{C_l^{H_2O}}\frac{i}{F}\right)C_l^M\right] \quad (7)$$

The Ohmic polarization is calculated using Ohm's law with the cell resistance calculated from Eq. (8); which accounts for the ionic resistance of the anode and cathode catalyst layers and the membrane.

$$R = \frac{1}{\kappa_e}\left[t_{Mem} + \frac{t_{ACL}}{\varepsilon_{e,ACL}^{1.5}} + \frac{t_{CCL}}{\varepsilon_{e,CCL}^{1.5}}\right] \quad (8)$$

II.5. Boundary conditions

The following boundary conditions were implemented to solve the governing equations (Eqs. (1) to (3)):

- No slip and normal flux conditions on all the channel walls
- A methanol concentration and normal oxygen flux of zero at the membrane – CCL interface
- A gauge pressure of 0 Pa at the anode and cathode channel outlets
- A known volume flow rate and reactant concentration at the AFF and CFF inlets

II.6. Mesh generation and solution procedure

The computational model is developed in COMSOL Multiphysics® 5.0, which is a commercially available finite element solver. The governing equations are implemented using the software's built-in modules ("Free and Porous Media Flow" for Eqs. (1) and (2), and "Transport of Diluted Species" for Eq. (3)), whereas the remaining constitutive equations are manually entered as user defined functions. An unstructured tetrahedral mesh of ~20 million elements, is used in this study. Three different segregated groups (one for each of the concentrations [methanol and oxygen], and one for the pressure and velocities) are configured to solve the set of equations. Each group is solved using the multifrontal massively parallel sparse (MUMPS) direct solver. Once the simulations are complete, the average quantities in each layer (e.g.: concentration, pressure and velocity) are outputted using probes. These quantities are used to analyze the simulation results as well to calculate of the fuel cell's electrochemical performance using Eqs. (4) - (8).

III. Results and Discussion

III.1. Pressure and Velocity

At an inlet flow rate to the stack of 10 mL/min (anode) and 1200 mL/min (cathode), the flow velocity between cells were found to be within 93% (anode) and 86% (cathode) of each other. This can be seen by the pressure drops between each stack cell shown in Fig. 2. The overall pressure drop for each stack's compartment was 26.2 Pa (anode) and 97.4 Pa (cathode). This pressure drop decreased from the cell closest to the stack's inlet, to the cell closest to the stack's outlet. Indicating that the bulk of the flow is through the cell closest to the stack's inlet, whereas the least amount of the bulk flow is through the cell nearest to the stack's outlet. It should further be noted that the anode's inlet and cathode's outlet occur within the same stack cell, and that the anode's outlet and cathode's inlet occur within the same cell. Therefore, special considerations will be needed for large-scale stacks to ensure that there is an adequate supply of methanol and oxygen to all stack cells.

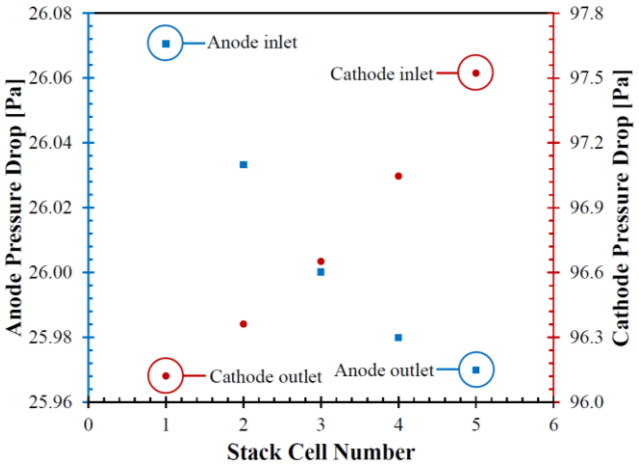

Fig. 2: Pressure drop across each cell's anode and cathode within the stack.

Within a given stack cell, it was found that there was little difference between the flow distribution between one anode parallel serpentine channel to the next (Fig. 3a); where the maximum pressure difference between the middle channel and the outer-most channel was 18 mPa at an inlet flow rate to the stack's anode of 10 mL/min. This small pressure difference seems to indicate that the effects of under-rib convection is small for the examined flow rate and that the flow within the ABL is diffusion-driven. However, within the cathode's parallel channel configuration (Fig. 3b), it was found that the channels within the middle of the CFF received the least amount of flow. For example, with an inlet flow rate to the stack's cathode of 1200 mL/min, the middle channels obtained a maximum velocity of 7 mm/s, whereas the outer-most channels obtained a maximum velocity of nearly 700 mm/s. It should be noted that the legend in Fig. 3b is condensed to allow for easier observation of the velocity differences between each channel. This difference in velocity distribution between channels is primarily attributed to the fact that at the cell's inlet, the bulk flow's momentum is directed along those first channels. As the flow travels along the top and bottom collector channels, the pressure difference becomes comparable, leading to very little flow being transported across the middle channels. Towards the cell's outlet, the pressure difference now becomes high due to its proximity to the cell's outlet, this forces the bulk flow to be transported through the last few channels. This indicates that the flow predominately travels along the first and last few channels. As will be discussed in the coming sections, this will yield better cell performance within these regions, with mass

transport limitations occurring within the centre of the MEA.

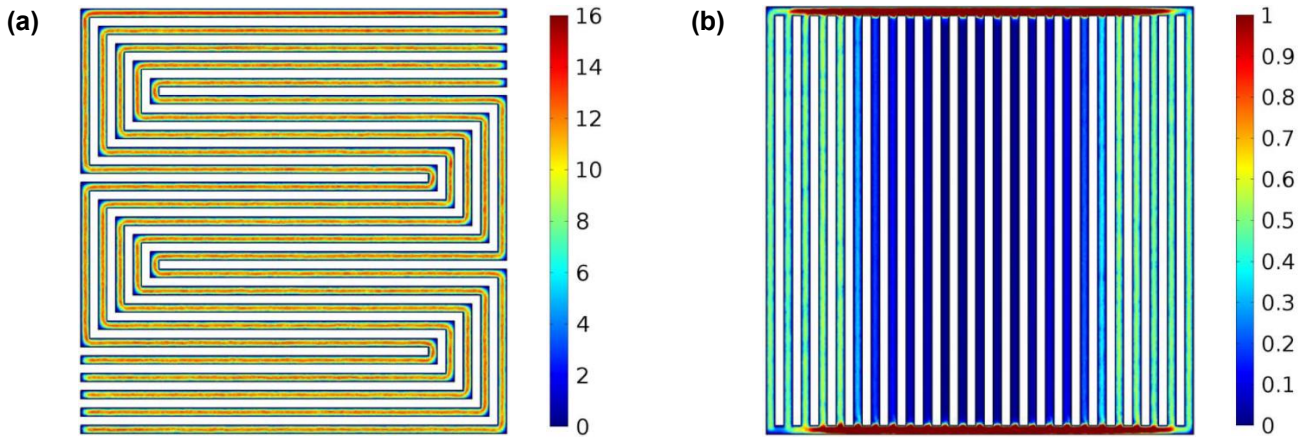

Fig. 3: The velocity within the anode [mm/s] and cathode [m/s] flow fields.

III.2. Methanol Concentration

As discussed in Section 4.1, the cell closest to the anode inlet received the greatest amount of flow, whereas the cell closest to the outlet received the least amount. As such, these cells had the most and least uniform methanol concentration distributions, respectively. However, the discussion in this section focuses on the cell closest to the anode inlet. Within this cell, the inlet anode stoichiometry for a single channel was approximately 0.2 (1 mL/min) and 2 (10 mL/min), as defined in Eq. 9 at a current density of 3000 A/m^2.

$$\xi_a^{MeOH} = \frac{\mathbf{u} \cdot C_{l,ch}^{MeOH} \cdot A_{ch}}{\frac{i}{6F} A} \tag{9}$$

However, the high diffusion resistances across the MEA caused the concentration of methanol at the ACL to rapidly diminish at low flow rates, as seen in Fig. 4. For instance, the mean methanol concentration at the ACL surface was 34.8 mol/m^3 (1 mL/min) and 384 mol/m^3 (10 mL/min), at a current density of 3000 A/m^2, and inlet concentration of 2000 mol/m^3. The low concentrations observed with the low flow rate caused high mass transport limitations, ultimately yielding lower cell voltages caused by higher anode activation polarizations.

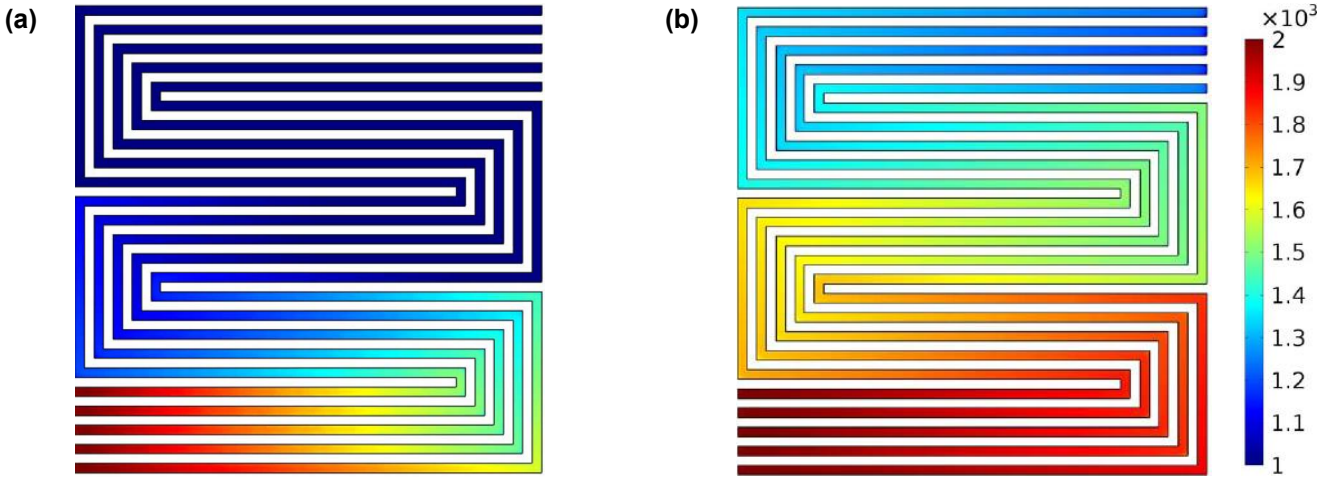

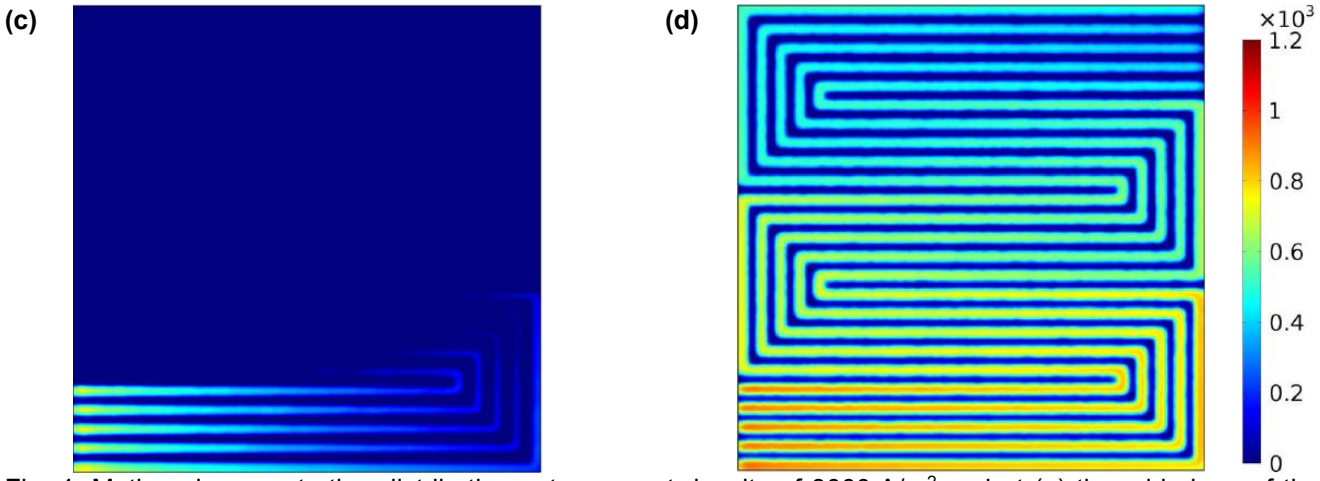

Fig. 4: Methanol concentration distributions at a current density of 3000 A/m^2 and at (a) the mid-plane of the anode flow field with an inlet flow rate of (a) 1 mL/min and (b) 10 mL/min; as well as at the anode catalyst layer surface with an inlet flow rate of (c) 1 mL/min and (d) 10 mL/min.

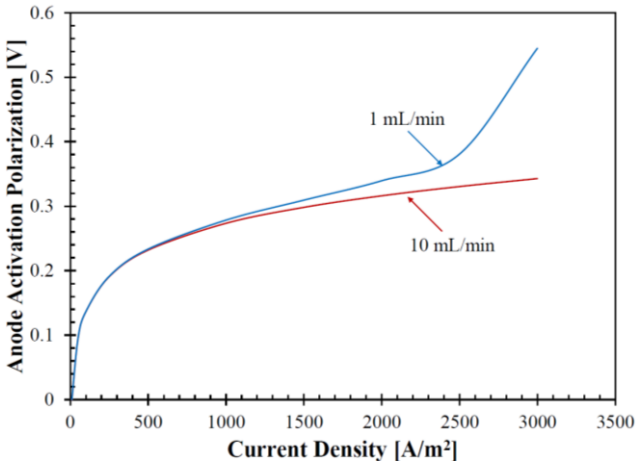

Fig. 5: The anode activation polarization for an anode inlet flow of 1 mL/min and 10 mL/min, both at a cathode inlet flow rate of 1200 mL/min.

As shown in Fig. 5 the lower flow rates yielded higher anode activation polarizations (i.e., 0.54 V [1 mL/min] and 0.34 V [10 mL/min]). The effect of the significant methanol depletion on the anode activation polarization within the 1 mL/min case (Fig. 4a,c), can be seen from the rapid increase in the activation polarization in Fig. 5. This rapid increase in indicative of the methanol oxidation reaction's 1st order reaction kinetics. It should be noted however, that higher anode flow rates also cause increased methanol permeation rates, i_{xover}; which can be detrimental to the CCL. For example, the highest i_{xover} which occurs at open circuit voltage (OCV) is 1187 A/m^2 (1 mL/min) and 3727 A/m^2 (10 mL/min).

III.3. Oxygen Concentration

The oxygen concentration at the CCL improved with increasing inlet flow rate, as shown in Fig. 6. For instance, the oxygen concentration at the CCL was 14.7 mol/m^3 (120 mL/min) and 33.2 mol/m^3 (1200 mL/min), a 69% and 30% decrease relative to the inlet concentration., respectively. Even with the increased methanol permeation rate, as discussed in the previous sub-section, the oxygen concentration at the CCL is still improved compared to the low flow rate case, because of the increased availability of reactants (stoichiometry of oxygen); which was able to effectively replenish the reduced oxygen.

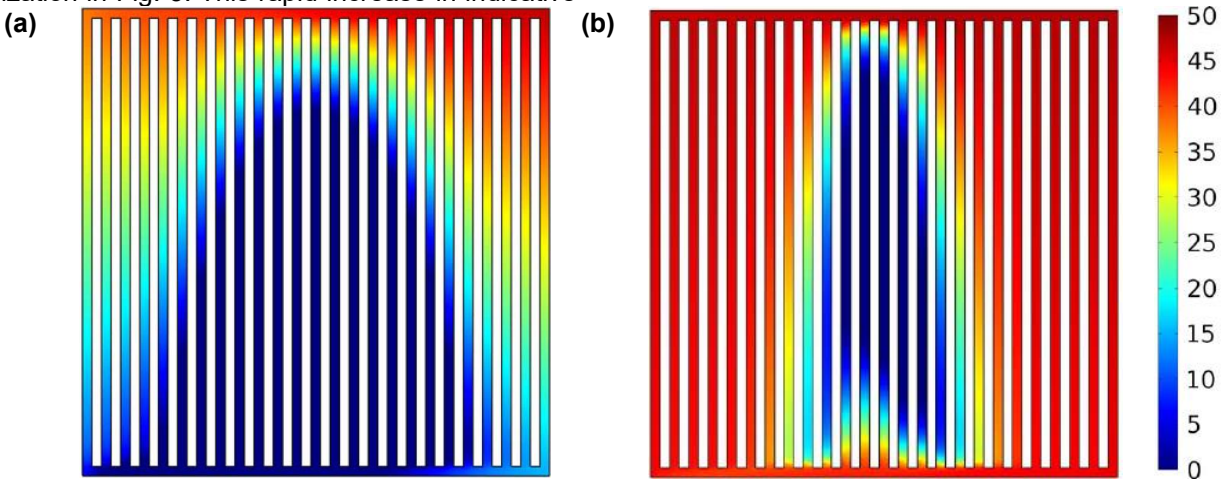

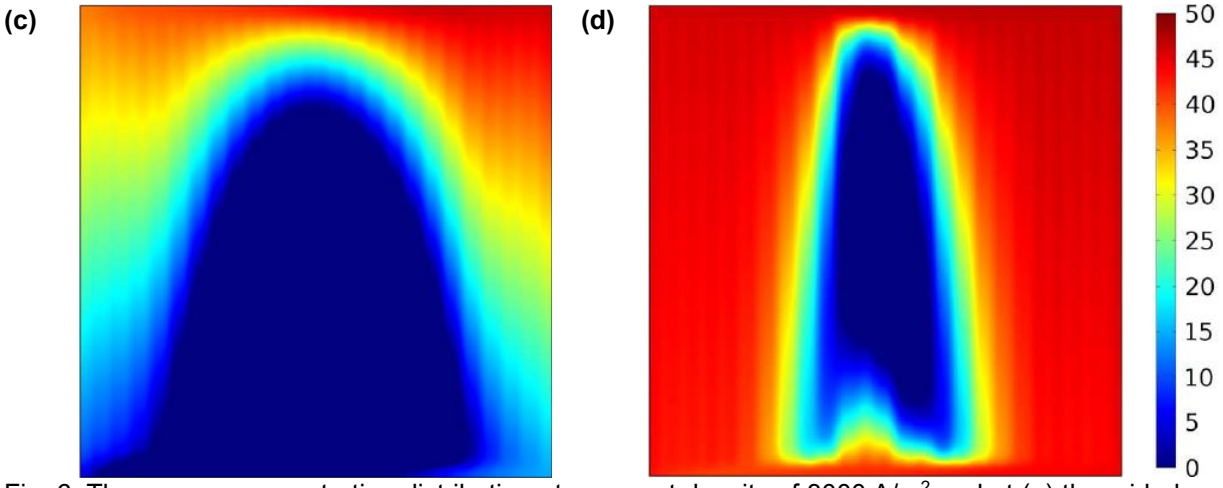

Fig. 6: The oxygen concentration distribution at a current density of 3000 A/m^2 and at (a) the mid-plane of the cathode flow field with an inlet flow rate of 120 mL/min and (b) 1200 mL/min; as well as, the cathode catalyst layer surface for a flow rate of (c) 120 mL/min and (d) 1200 mL/min.

The differences in cathode activation polarization are shown in Fig. 7, between the 1 and 10 mL/min (anode) flow rates, and the 120 and 1200 mL/min (cathode) flow rates. This visualization provides a clear indication of the relative importance between the cathode flow rate and the amount of methanol permeation to the cathode. For instance, increased methanol flow rates cause an increase in methanol permeation, yielding a higher cathode activation polarization. However, the greatest impact occurred when the cathode flow rate was reduced to 120 mL/min (anode flow rate set to 10 mL/min). Because of the lower cathode stoichiometry, the oxygen concentration at the CCL diminished, causing an increased cathode activation polarization.

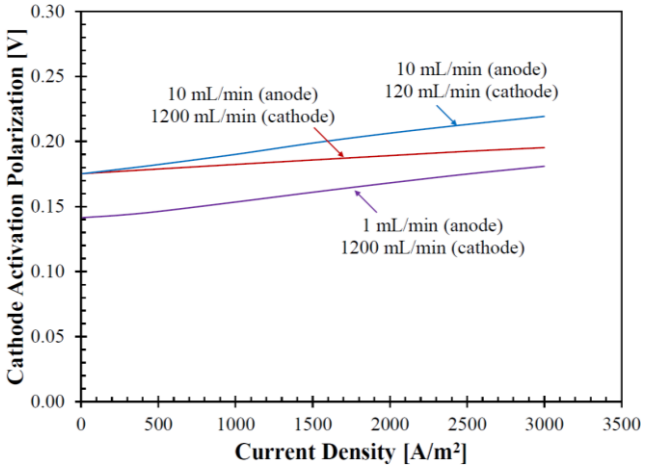

Fig. 7: Comparison between the cathode activation polarization for different anode and cathode inlet flow rate configurations.

IV. Conclusions

In this study, a 3D modelling approach is proposed, and applied to a 5-cell direct methanol fuel cell (DMFC) short-stack. The mass and species transport were solved in a 3D manner; whereas the electrochemical performance of the fuel cell was solved analytically. To solve the modelling equations, equations originating from the conservation of mass, momentum and chemical species and the electrochemical relations were coupled and solved using a numerically available software, namely Comsol Multiphysics. The main conclusions derived from this study are as follows:

- The stack cell compartments (anode and cathode) closest to their respective inlets received the greatest amount of flow, whereas the cells closest to their respective outlets received the least amount of flow.
- Under the examined operating conditions, the pressure difference between adjacent parallel serpentine channels are very small causing little under-rib convection. This allows for the species transport to be efficiently modeled as diffusion-dominated within the BLs.
- Decreased cathode activation polarizations can be achieved with a decreased methanol flow rate.
- Parallel channels are susceptible to locally low flow rates within the middle channels. This can yield significant mass transport limitations within these regions.

Acknowledgements

The funding for this project was received from the European Union's Horizon 2020 research and innovation programme under the Marie Sklodowska-Curie grant agreement No. 661579.

Reference

Argyropoulos P., Scott K., Taama W. M., Modeling flow distribution for internally manifolded direct methanol fuel cell stacks, Chemical Engineering & Technology, 23(11), 985-995, (2000).

Barbir F., PEM fuel cells: theory and practice, Academic Press. (2012).

Brandão L., Rodrigues J., Madeira L. M., Mendes A., Methanol crossover reduction by Nafion modification with

palladium composite nanoparticles: Application to direct methanol fuel cells, International Journal of Hydrogen Energy, 35(20), 11561-11567, (2010).

Casalegno A., Santoro C., Rinaldi F., Marchesi R., Low methanol crossover and high efficiency direct methanol fuel cell: the influence of diffusion layers, Journal of Power Sources, 196(5), 2669-2675, (2011).

Chang P., Kim G. S., Promislow K., Wetton B., Reduced dimensional computational models of polymer electrolyte membrane fuel cell stacks, Journal of Computational Physics, 223(2), 797-821, (2007).

Colpan C. O., Ouellette D., Glüsen A., Müller M., Stolten D., Reduction of methanol crossover in a flowing electrolyte-direct methanol fuel cell, International Journal of Hydrogen Energy, (2017).

Fang L., Di L., Ru Y. A dynamic model of PEM fuel cell stack system for real time simulation, In Power and Energy Engineering Conference, APPEEC 2009. Asia-Pacific (pp. 1-5). IEEE, (2009).

Kablou Y., Hydrodynamic Modelling and Experimental Analysis of FE-DMFC Stacks, PhD Thesis, Carleton University, Ottawa, Canada, 2012.

Kong X., Khambadkone A. M., Modeling of a PEM fuel-cell stack for dynamic and steady-state operation using ANN-based submodels, IEEE Transactions on Industrial Electronics, 56(12), 4903-4914, (2009).

Kvesić M., Reimer U., Froning D., Lüke L., Lehnert W., Stolten D., 3D modeling of a 200 cm 2 HT-PEFC short stack. International Journal of Hydrogen Energy, 37(3), 2430-2439, (2012).

Liu G., Zhou H., Ding X., Li X., Zou D., Li X., Wang X., Lee, J. K., Effect of fabrication and operating parameters on electrochemical property of anode and cathode for direct methanol fuel cells, Energy Conversion and Management, 122, 366-371, (2016).

Liu Z., Mao Z., Wang C., Zhuge W., Zhang Y., Numerical simulation of a mini PEMFC stack. Journal of Power Sources, 160(2), 1111-1121, (2006).

Mondal S., Soam S., Kundu P. P., Reduction of methanol crossover and improved electrical efficiency in direct methanol fuel cell by the formation of a thin layer on Nafion 117 membrane: Effect of dip-coating of a blend of sulphonated PVdF-co-HFP and PBI, Journal of Membrane Science, 474, 140-147, (2015).

Musio F., Tacchi F., Omati L., Stampino P. G., Dotelli G., Limonta S., Davide B., Grassini P., PEMFC system simulation in MATLAB-Simulink® environment, International Journal of Hydrogen Energy, 36(13), 8045-8052, (2011).

Ozden A., Ercelik M., Ouellette D., Colpan C. O., Ganjehsarabi H., and Hamdullahpur F., Designing, modeling and performance investigation of bio-inspired flow field based DMFCs, International Journal of Hydrogen Energy, (2016), doi: 10.1016/j.ijhydene.2017.01.007.

Philipps S. P., Ziegler C., Computationally efficient modeling of the dynamic behavior of a portable PEM fuel cell stack, Journal of Power Sources, 180(1), 309-321, (2008).

Scott K., Argyropoulos P., Taama W. M., Modelling transport phenomena and performance of direct methanol fuel cell stacks, Chemical Engineering Research and Design, 78(6), 881-888, (2000).

Seo S. H., Lee C. S., A study on the overall efficiency of direct methanol fuel cell by methanol crossover current, Applied Energy, 87(8), 2597-2604, (2010).

Shimpalee S., Ohashi M., Van Zee J. W., Ziegler C., Stoeckmann C., Sadeler C., Hebling C., Experimental and numerical studies of portable PEMFC stack, Electrochimica Acta, 54(10), 2899-2911, (2009).

Wang R., Qi L., Xie X., Ding Q., Li C., Ma C. M., Modeling of a 5-cell direct methanol fuel cell using adaptive-network-based fuzzy inference systems, Journal of Power Sources, 185(2), 1201-1208, (2008).

Zelenay P., Advanced Materials and Concepts for Portable Power Fuel Cells, US DOE Hydrogen Program Annual Merit Review and Peer Evaluation, (2012).